Materials Chemistry and Physics 366 (2026) 132958

Contents lists available at ScienceDirect

Materials Chemistry and Physics

journal homepage: www.elsevier.com/locate/matchemphys

Bioactive glasses co-doped with zinc and magnesium: Bioactivity, ion release, and antimicrobial activity against Gram-positive and Gram-negative bacteria

D. Bellucci [a,*], F. Basoli [b], S. De Micco [a], E. D'Alessandro [b], S. Grasso [c], M. Giovanetti [c], M. Trombetta [b], V. Cannillo [a,**]

[a] Dipartimento di Ingegneria "Enzo Ferrari", Università di Modena e Reggio Emilia, Via P. Vivarelli 10, 41125, Modena, Italy
[b] Dipartimento di Ingegneria, Università Campus Bio-Medico di Roma, Via Alvaro del Portillo, 21, 00128, Rome, Italy
[c] Dipartimento di Scienze e Bio-Tecnologie, Università Campus Bio-Medico di Roma, Via Alvaro del Portillo, 21, 00128, Rome, Italy

HIGHLIGHTS

- Novel Zn/Mg bioactive glasses with tunable composition were developed.
- Small compositional changes strongly affected glass reactivity and ion release.
- Zn-rich glasses exhibited enhanced antibacterial activity through sustained ion release.
- One composition (Roma2) effectively inhibited both Gram-negative and Gram-positive bacteria.
- Roma2 emerged as the most promising multifunctional bioactive glass formulation.

ARTICLE INFO

Keywords:
Bioactive glasses (BGs)
Zinc doping
Magnesium doping
Antibacterial properties

ABSTRACT

Bioactive glasses (BGs) are widely studied for their ability to bond with tissues, release biologically active ions, and exhibit antimicrobial activity. In this study, a series of Zn- and Mg-containing BGs were synthesized via the melt-quench method, varying the relative contents of ZnO and MgO. Structural and thermal properties were characterized using X-ray diffraction, differential thermal analysis, and heating microscopy, while their in vitro bioactivity was preliminarily assessed through immersion in Simulated Body Fluid. Ion release was quantified by Inductively Coupled Plasma Mass Spectrometry with Triple Quadrupole, and antimicrobial activity was tested against *Escherichia coli (E. coli)* and *Staphylococcus aureus (S. aureus)*. The results demonstrate that compositional variations influence the physicochemical behavior, ion-release characteristics, in vitro bioactivity, and antibacterial performance of BGs. In particular, Zn content played a key role: glasses in which Zn acted mainly as a network modifier showed enhanced reactivity, sustained Zn^{2+} release, and strong alkalinization of the medium, which correlated with improved antibacterial activity. Notably, one of the developed formulations (Roma2) exhibited a highly favorable combination of structural stability, ion-release behavior, in vitro bioactivity, and antibacterial efficacy against both Gram-negative and Gram-positive bacteria. Overall, these findings highlight the potential of Zn- and Mg-doped BGs as multifunctional biomaterials for bone-related applications requiring antibacterial functionality.

1. Introduction

Bioactive glasses (BGs) are a class of biomaterials known for their ability to bond with bone and soft tissues, stimulate regeneration, and release biologically active ions. Since their introduction by Larry L. Hench in 1969 with the composition of 45S5 Bioglass® (46.1 mol% SiO_2, 26.9 mol% CaO, 24.4 mol% Na_2O, and 2.6 mol% P_2O_5), BGs have been extensively studied and applied in orthopedics, dentistry, and

* Corresponding author.
** Corresponding author.
E-mail addresses: devis.bellucci@unimore.it (D. Bellucci), valeria.cannillo@unimore.it (V. Cannillo).

https://doi.org/10.1016/j.matchemphys.2026.132958
Received 2 February 2026; Received in revised form 16 July 2026; Accepted 25 July 2026
Available online 28 July 2026

tissue engineering [1]. According to their chemical composition, BGs can be broadly classified into silicate-, borate-, and phosphate-based systems, each characterized by distinct dissolution behavior, bioactivity, and ion-release profiles that make them suitable for different biomedical applications [2,3]. Among these, silicate-based BGs are by far the most widely investigated owing to their high bioactivity, compositional flexibility, and proven clinical success.

Biomaterials are typically classified into three generations [4]. The first generation was developed with the aim of producing bioinert and biocompatible materials that minimized adverse tissue reactions. A decisive breakthrough occurred in the late 1960s, when Hench demonstrated that a synthetic material could bond directly with living bone, paving the way for second-generation biomaterials characterized by bioactivity and controlled biodegradability. Subsequently, the concept of third-generation biomaterials emerged from the convergence of bioactive and resorbable systems. Molecularly tailored biomaterials – including BGs, composites, hybrid systems, and macroporous foams – are designed to interact at the molecular level, activate genes, guide cell behavior, and promote tissue regeneration [1]. Although BGs are considered an emblematic example of second-generation biomaterials, they can also be engineered to function as third-generation biomaterials when processed in specific forms, such as powders, with properties tailored for particular applications, including angiogenic, osteogenic, or antibacterial activity [5]. Besides composition, the synthesis route, including conventional melt-quench and sol-gel processing, plays a key role in determining the glass structure, homogeneity, porosity, ion-release behavior, and ultimately its biological performance. Consequently, both composition and processing must be carefully tailored to the intended biomedical application [6].

Two main strategies have been developed to achieve antibacterial performance [7], a key property for biomedical materials. The first involves incorporating metallic or alkaline ions with antimicrobial activity, while the second focuses on designing BGs with high dissolution rates of alkali and alkaline-earth ions, which locally raise the pH and create an environment hostile to many pathogens. Several studies have reported a correlation between the antibacterial properties of BGs and their corresponding pH levels [8]. A major milestone in this field was the development of the composition S53P4, commercially known as BonAlive® (53.8 mol% SiO_2, 21.8 mol% CaO, 22.7 mol% Na_2O, 1.7 mol% P_2O_5), the first BG with proven antibacterial properties [9]. S53P4 has demonstrated broad-spectrum efficacy against both aerobic and anaerobic bacteria [9]. More recently, the development of multifunctional antibacterial biomaterials has attracted increasing attention, with antimicrobial efficacy being attributed to the synergistic contribution of multiple mechanisms, including therapeutic ion release, local pH increase, inhibition of bacterial adhesion, and prevention of biofilm formation [10].

Several therapeutic ions, including strontium (Sr), copper (Cu), silver (Ag), zinc (Zn), and magnesium (Mg), have been incorporated into BGs to confer specific biological functionalities, such as osteogenic, angiogenic, or antibacterial activity [11]. Among these, zinc [12,13] and magnesium [14] are two of the most extensively investigated, since both ions are naturally present in the human body and play essential physiological roles. However, several studies report that the antimicrobial property of Mg is still debated and, in some cases, inconsistent, whereas Zn has been consistently associated with higher inhibition of *E. coli* and *S. aureus* [15–17]. Besides their antibacterial relevance, both ions have been extensively investigated for their beneficial effects on bone metabolism, as demonstrated by numerous in vitro and *in vivo* studies. Zn has been reported to: (i) stimulate osteoblast proliferation and differentiation; (ii) upregulate genes involved in angiogenesis and anti-inflammatory processes [18]; (iii) stimulate alkaline phosphatase (ALP) production [18]; (iv) inhibit osteoclast activity [19]; and (v) exert a broad-spectrum antibacterial effect against Gram-negative and Gram-positive bacteria [20,21]. Zn contributes to the antibacterial activity of BGs through multiple mechanisms [22–24], including reducing the ability of bacteria to tolerate acidic by-products generated during glycolysis [25,26]. In addition, Zn can disrupt bacterial metal homeostasis, leading to increased oxidative stress via reactive oxygen species (ROS) generation [20,24]. Beyond its biological and antibacterial functions, Zn also influences the structural organization and dissolution behaviour of BGs [12,13]. Literature suggests that when ZnO is incorporated into the composition of the BGs, it acts primarily as a network modifier, decreasing the silicate network connectivity (NC) and increasing the number of non-bridging oxygens [27]. This structural effect enhances the early dissolution rate and the release of Zn and Ca ions, thereby influencing the nucleation of Ca–P phases and the local changes in pH [27].

On the other hand, the impact of Zn on the formation of a hydroxyapatite (HAp) layer on the surface of BGs – one of the most widely used indicators of their in vitro bioactivity – remains debated [14,28]. Conflicting findings have been reported, particularly regarding Zn content: several studies have indicated that Zn concentrations above 10 mol% can negatively affect glass bioactivity by slowing HAp formation [14,22,29]. Unlike calcium, which in HAp is typically octahedrally coordinated with relatively long Ca–O bonds, Zn often exhibits shorter Zn–O bonds and preferential tetrahedral coordination within silicate glass networks [27]. These structural characteristics may favor the formation of stable zinc phosphate species, which are structurally incompatible with the HAp lattice [27]. Consequently, Zn may compete with calcium and interfere with phosphate incorporation into HAp, thereby delaying its nucleation and growth on the BG surface [27].

Magnesium (Mg), the fourth most abundant cation in the human body, is also essential for bone health [14]. It contributes to bone mineralization, supports osteoblast activity, and stabilizes newly formed bone tissue [14]. When incorporated into BGs, Mg enhances biocompatibility, promotes osteogenesis, and supports cellular differentiation [30]. Moreover, Mg-doped BGs exhibit improved dissolution behavior in physiological environments, facilitating ion exchange and enhancing biological responsiveness [14]. At the same time, Mg has also been reported to retard the crystallization of the initially formed amorphous calcium-phosphate layer, thereby delaying the formation of crystalline HAp during the early stages of immersion in physiological media [31].

When combined, Zn and Mg can provide synergistic effects [32–34]: for example, in co-doped systems, the simultaneous incorporation has been shown to stimulate osteogenesis, preserve zinc's antibacterial properties, and maintain controlled degradation rates [14].

Based on these considerations, we hypothesized that small variations in the Zn/Mg ratio would significantly influence the structural characteristics, thermal behavior, ion-release profile, in vitro bioactivity, and antibacterial performance of melt-derived bioactive glasses. Accordingly, the aims of the present study were to (i) synthesize a series of Zn/Mg-containing bioactive glasses with different compositions, (ii) investigate the influence of composition on their structural and thermal properties, (iii) evaluate their ion-release behavior and in vitro bioactivity in SBF, and (iv) assess their antibacterial activity against both Gram-positive and Gram-negative bacteria. The results demonstrate that even small compositional variations, particularly in Zn content, significantly affect these properties and the overall antibacterial performance of the investigated glasses.

2. Materials and methods

2.1. Preparation of the bioactive glasses (BGs)

Six novel BGs were produced using the melt-quench technique, a method previously employed for the synthesis of other BGs [35]. Finely powdered raw materials (SiO_2, $Ca_3(PO_4)_2$, $CaCO_3$, Na_2CO_3, $MgCO_3$, ZnO, all reagent grade - Carlo Erba Reagenti, Rodano-Milano, Italy) were weighed and mixed in a laboratory rotary mixer (M63a4-Motori Elettrici Carpanelli, Bologna, Italy) for 4 h to ensure homogeneity. The mixture was then transferred into a platinum crucible and subjected to

the following thermal treatment: heating from room temperature to 1100 °C at 10 °C/min; decarbonation at 1100 °C for 1.5 h to ensure the complete decomposition of the carbonate precursors before melting; heating from 1100 °C to 1450 °C at 10 °C/min; and holding at 1450 °C for 1 h to obtain a homogeneous melt. The molten material was then rapidly quenched in water to form a glass frit, which was subsequently dried at 110 °C for 12 h, finely ground for 40 min in a porcelain jar, and sieved to obtain particles smaller than 63 μm. The compositions of the BGs, expressed in mol%, are reported in Table 1.

2.2. Particle size analysis

To determine the particle size distribution, diluted sample suspensions (0.1% w/v) of the glass powders were prepared and analyzed using a Split-flow Thin Cell Field-Flow Fractionation (SdFFF) system. A 50 mL Rheodyne loop valve was used for sample injection, while a PN1121 HPLC pump (Postnova Analytics, Germany) was used to deliver the eluent. The fractionated particles were monitored by a UV/Vis detector (Spectra SERIES UV100, Thermo Separation Products) operating at a fixed wavelength of 254 nm. Instrument control and data acquisition were managed using the SPIN 1409 software, with subsequent data processing performed via the FFF ANALYSIS program – both provided by Postnova Analytics. The mobile phase consisted of a 0.01% (w/v) solution of Triton X-100 in Milli-Q water (Millipore S.p.A., Vimodrone, Milan, Italy), flowing at 2 mL/min. The obtained fractograms were converted into particle size distribution, assuming a bulk density of 1.3 g/mL for all samples.

2.3. Analysis of the crystalline phases

X-ray diffraction (XRD) analysis was carried out to investigate the presence and nature of the crystalline phases developing in the produced samples and after exposure to SBF (see the next paragraphs). The measurements were performed using an X-Ray Diffractometry (XRD: X'Pert PRO; Panalytical, Almelo, the Netherlands) equipped with a Cu-kα X-ray source ($\lambda = 1.5406$ Å), operating at 40 kV and 40 mA. Data were collected in the 2θ range of 10° to 70°, with a step size of 0.017°. The scan was performed in continuous mode using a PIXcel3D detector. Samples were finely ground and deposited on a sample holder to ensure a flat and homogeneous surface. In order to investigate which crystalline phases form following prolonged heat treatment, the glasses Roma1, Roma2, and Roma5 – i.e., those found to be most interesting in terms of antibacterial activity – were treated at 700 °C and 750 °C for 3 h, with a heating rate of 10 °C/min. In this case as well, the development of crystalline phases was studied by XRD.

2.4. Thermal analysis

The thermal properties of the BG powders were investigated using Differential Thermal Analysis (DTA). For this purpose, ~30 mg of each sample were placed in a platinum crucible and heated from room temperature up to 1200 °C at a constant rate of 20 °C/min using a STA 429 CD analyzer (Netzsch-Gerätebau GmbH, Selb, Germany). The resulting DTA curves were used to identify characteristic temperatures of the BGs, including: glass transition temperature (T_G), onset crystallization temperature (T_{C_onset}), and peak crystallization temperature (T_C).

Additionally, a heating microscope (HM) was used to monitor the behavior of the glass powders over a wider temperature range, from room temperature to 1600 °C, with a heating rate of 10 °C/min. This analysis was conducted using a Misura 3.32 equipment (Expert System Solutions, Modena, Italy). The results allowed the determination of the sintering temperature (T_S) and the melting temperature (T_M) of the BGs.

The combined use of DTA and HM was specifically selected because these complementary techniques provide the characteristic temperatures relevant to glass processing and sintering, which were the primary focus of the present thermal investigation.

Table 1
Composition in mol% of the six BGs produced in the present study.

Sample	SiO_2	P_2O_5	CaO	Na_2O	MgO	ZnO
Roma1	47.2	2.6	25.6	14.6	5	5
Roma2	47.2	2.6	20.6	14.6	5	10
Roma3	47.2	2.6	20.6	19.6	5	5
Roma4	47.2	2.6	20.6	9.6	5	15
Roma5	53.8	1.7	16.8	17.7	5	5
Roma6	53.8	1.7	16.8	12.7	5	10

2.5. In vitro bioactivity evaluation in SBF

To evaluate the bioactivity of the BG powders, an in vitro semi-dynamic test was carried out by soaking them in Simulated Body Fluid (SBF), following the procedure established by Kokubo et al. [36]. Specifically, 0.3 g of glass powders were added to 20 mL of SBF and incubated at 37 °C for different time intervals (1, 3 and 7 days). The solid-liquid ratio was selected according to the protocol reported by Jones et al. [37]. The pH of the solution was regularly monitored at the same temperature, and the entire volume of SBF was refreshed every 48 h to maintain consistent conditions. The initial pH was 7.4, in accordance with the Kokubo protocol. At each interval, the powders were collected, washed with distilled water, and dried at room temperature for ~48 h. The surface morphology and elemental composition of the treated samples were then analyzed using SEM-FEG (SEM, Scanning Electron Microscopy) with a Field Emission Gun (FEG) (Nova NanoSEM 450, FEI-ThermoFisher Scientific, Eindhoven, The Netherlands) and X-ray energy dispersive spectroscopy (EDX) (Quantax-200, Bruker Nano GmbH, Berlin, Germany). Moreover, the powders after 7 days of immersion were studied by means of XRD to identify the possible presence of crystalline precipitates.

2.6. Measurement of ion release

To evaluate the release of ionic species from the BGs powders, an in vitro dissolution test was conducted in Milli-Q distilled water. This medium was selected instead of physiological solutions (e.g., SBF or DMEM) to evaluate the intrinsic dissolution behavior of the glasses under controlled conditions, minimizing precipitation phenomena and interactions with ions already present in the surrounding solution. In each test, 0.4 g of powder was suspended in 25 mL of water and maintained at 37 °C under static conditions. This solid-to-liquid ratio (16 mg/mL) was selected to be consistent with that adopted for the SBF tests (15 mg/mL), ensuring comparable experimental conditions. After the predefined immersion period, the suspensions were filtered using 0.45 μm pore size membranes to remove any residual nanoparticles from the solution. The resulting filtrates were analyzed using Inductively Coupled Plasma Mass Spectrometry with Triple Quadrupole (iCAP TQ ICP-MS, Thermo Fisher Scientific, Bremen, Germany).

To minimize non-spectral interferences and ensure accurate quantification, the method incorporated internal standardization with scandium. A calibration curve was constructed using certified ionic reference standards, and the filtered sample solutions were analyzed. All measurements were performed in triplicate, and the ion concentrations are reported as mean values.

2.7. Antimicrobial study

2.7.1. Bacterial strains

To evaluate the antimicrobial activity of the BG powders, tests were conducted on both Gram-negative and Gram-positive bacterial strains. Freeze-dried *Escherichia coli* (Migula) Castellani and Chalmers, used as the Gram-negative model strain (ATCC 25922), was obtained from ATCC (Manassas, VA, USA). Freeze-dried *Staphylococcus aureus* (ATCC

25923), used as the Gram-positive model strain, was also obtained from ATCC (Manassas, VA, USA). Each bacterial strain was revived by overnight incubation in Luria-Bertani (LB) medium at 37 °C under agitation at 75 rpm. After revival, the cultures were further enriched by transferring the bacterial suspension into 25 mL of fresh liquid LB medium and incubating at 37 °C for 12 h. Before the antimicrobial assay, bacterial suspensions were adjusted to an initial concentration of about 1 × 103 CFU/mL using sterile LB medium. The inoculum concentration was verified by serial dilution and colony counting on LB agar plates.

2.7.2. Preparation of the eluate for antimicrobial testing

Prior to testing, all BG samples were placed in Petri dishes and sterilized under UV light for 1 h on each side to ensure sterility. Extracts were prepared by immersing the sterilized materials in centrifuge tubes containing LB culture medium at a final concentration of 200 mg/mL, following the ISO 10993-12 guidelines. The samples were incubated at 37 °C for 72 h under gentle agitation to allow ion release. The resulting eluates were centrifuged at 1,200 × g for 15 min and the supernatant was collected and stored at 4 °C until use.

2.7.3. Antimicrobial testing

For the antimicrobial test, bacterial suspensions were exposed to eluates obtained from BGs with different compositions and dopant concentrations, as reported in Table 1. The bacterial suspension and each BG extract were mixed at a ratio of 1:9 and then a volume of 500 μL was plated onto LB agar using the spread plate method. Appropriate controls were also included in each experiment. A bacterial growth control consisted of bacterial suspension incubated with sterile LB medium without BG extract. A sterility control consisted of sterile LB medium and/or BG extract without bacterial inoculum. Plates were incubated at 37 °C for 18 h, after which visible colonies were counted. The number of viable bacteria was expressed as colony-forming units per millilitre (CFU/mL) according to the following equation:

$$CFU \Big/ mL = \frac{N \times D}{V}$$

where N is the number of colonies counted, D is the dilution factor, and V is the plated volume in millilitres.

The antibacterial activity of each BG extract was calculated relative to the bacterial growth control as:

$$Antibacterial\ efficacy\ (\%) = \left(1 - \frac{CFU_{sample}}{CFU_{control}}\right) \times 100$$

where $CFU_{control}$ represents the viable bacterial count obtained from the growth control and CFU_{sample} represents the viable bacterial count after exposure to the BG extract.

All experiments were performed in duplicate to ensure reproducibility and reliability of the results. Data were expressed as mean ± standard deviation.

3. Results and discussion

3.1. Particle size analysis

The graph in Fig. 1 shows, as an example, the particle size distribution of the Roma5 sample, which was analyzed after the melt-quench process, followed by grinding and sieving to a size below 63 μm.

All the investigated glasses exhibited comparable particle size distributions because they were processed using the same grinding and sieving procedure; therefore, only one representative distribution is reported for brevity. The results show a unimodal distribution, with most particles ranging from approximately 2 to 40 μm. The characteristic diameters D10, D50, and D90 were also determined. D10 = 2.735 μm indicates that 10% of the particles have a diameter smaller than 2.735 μm. D50 = 9.328 μm represents the median particle size, meaning that half of the particles are smaller than this value. D90 = 33.083 μm indicates that 90% of the particles have a diameter below 33.083 μm. The peak of the distribution is close to D50, at around 9–10 μm, confirming that this is the most frequent particle size in the sample. The volume percentage gradually decreases on both sides of the peak, forming a nearly symmetrical, bell-shaped curve. This confirms that the sieving step was effective in removing larger particles and producing a relatively narrow and controlled size distribution.

3.2. Thermal analysis

HM analysis provided the characteristic thermal events of the glasses, including sintering, softening (onset of sample collapse), and melting temperatures. In some cases, hemispherical and/or spherical temperatures were also recorded. As a representative example, Fig. 2

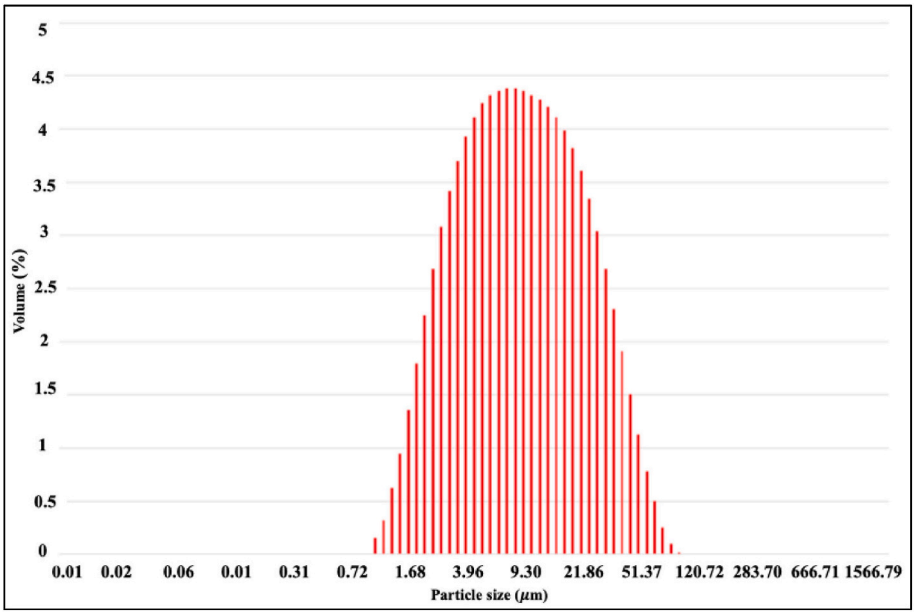

Fig. 1. Particle size distribution in the Roma5 sample.

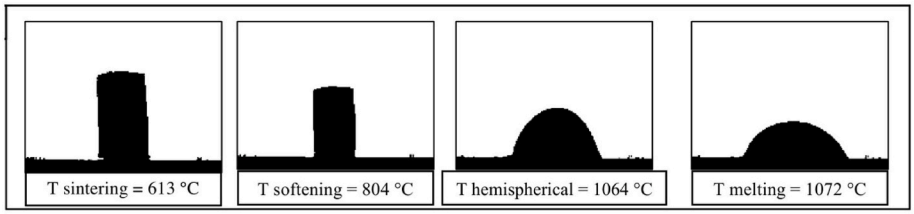

Fig. 2. HM analysis of the Roma1 sample, shown here as a representative example of the results obtained for the different samples.

shows the HM images obtained for the Roma1 sample. The sequence of morphological changes during heating was qualitatively similar for all the investigated compositions; therefore, only one set of images is reported, whereas the characteristic temperatures determined for all the glasses are summarized in Table 2. However, HM mainly indicates the onset of shrinkage and does not fully determine the optimal sintering conditions, which depend on viscosity and crystallization kinetics. Further studies are needed to better define the sintering window of the produced BGs. Among these, Roma6 exhibited the highest sintering temperature. The melting temperatures (T_m) of the studied BGs (~1029-1101 °C) were slightly lower than that of 45S5 (1165-1193 °C) [23,33]. This effect can be attributed to the specific proportions of Ca, Mg, Zn, and Na, which promote network depolymerization, thereby lowering T_m and shifting crystallization to higher temperatures, ultimately broadening the processing window.

Fig. 3 shows the results of the DTA analysis. The DTA curves of the glass powders show the onset crystallization temperatures (T_{c_onset}) between 620 °C and 790 °C, with the main exothermic peaks associated with crystallization appearing in the range 680–850 °C. The glass transition temperatures (T_G) generally occurred between 520 °C and 570 °C. For comparison (see Table 2), 45S5 Bioglass® typically shows $T_G \approx$ 520-549 °C and T_c in the interval 600–750 °C, a value that varies depending on the particle size distribution and the applied thermal treatment [23,33], while the glasses investigated here display similar T_G values but higher T_c, leading to wider processing windows ($T_c - T_G$) [38–40].

In 45S5, crystallization is usually influenced by the mobility of modifier cations and by the ability of oxides to promote the nucleation of ordered phases [41]. The presence of phosphorus in significant amounts contributes to the early onset of crystallization. In the Mg–Zn containing BGs, the structural role of these ions modifies the crystallization pathway. As reported by Wetzel et al. [42], Mg and Zn can partially substitute Ca in the network, generating random substitutional mixing among divalent cations. This substitution is driven by entropic stabilization and alters the balance between modifier and network formers. Mg and Zn primarily act as modifiers, and this can be related to the distinct bonding characteristics of Mg–O, which, compared with Ca–O, may facilitate a higher disruption of Si–O–Si and P–O–P bridges, thereby increasing the fraction of non-bridging oxygens [43,44]. In particular, Zn may act as either an intermediate [45] or a modifier [46]. In tetrahedral coordination, Zn typically behaves as a weak network modifier; in this configuration, its bonding promotes network depolymerization, an effect that is generally more pronounced than that induced by Ca but depends on the overall glass composition [41]. However, the literature is not always consistent on the effect of Zn and Mg. In some studies, ZnO and MgO have been shown to reduce T_G and T_c. This effect may be attributed to the weaker network-forming ability of Mg and Zn [43,47]. On the other hand, some works report that partial substitution of Ca with Zn or Mg can increase the processing window and improve sintering behavior [25,40]. These discrepancies are related to the dual structural role of Zn and Mg, which can act differently depending on their concentration and the presence of other network modifiers or formers. A wider window for these BGs (*Roma1-Roma6*) indicates a reduced tendency for early crystallization and improved workability during viscous-flow sintering [28]. The comparison of temperatures between 45S5 Bioglass® and the novel BGs produced in this study is reported in Table 2.

Table 2
– Comparison of glass transition (T_G), crystallization onset (T_{C_onset}), crystallization (T_C), melting (T_m), and sintering (T_S) temperatures between 45S5 Bioglass® [23] and the novel BGs produced in this study.

	Rate (°C/min)	T_G (°C)	T_{C_onset} (°C)	T_C (°C)	T_m (°C)	T_S (°C)
45S5 Bioglass®	*20*	*520*	*560*	*638*	*1193*	*594*
Roma1	20	553	688	763	1072	613
Roma2	20	524	629	684	1092	581
Roma3	20	550	730	800	1101	617
Roma4	20	570	769	819	1101	614
Roma5	20	540	695	770	1029	611
Roma6	20	564	789	844	1034	631

3.3. Phase analysis

Fig. 4 presents the XRD analysis results of the as-produced BGs. As expected, all spectra show a diffuse halo in the range of 20–35° 2θ, confirming that the samples are essentially amorphous and lack long-range crystalline order. Besides the amorphous halo, very small recurrent peaks can be observed (e.g., around 27°, 35°, 43°, and 57° 2θ); however, their intensity is extremely low and close to the background noise level. As a result, no crystalline phases were detected, indicating that the addition of Mg and Zn, as well as the variations in Ca and Na content, did not promote crystallization under the present melting and quenching conditions. Preserving an amorphous structure is particularly relevant for bioactivity, as it enhances ion release and accelerates the formation of a HAp layer upon exposure to physiological environments.

Roma1, Roma2, and Roma5 – the BGs that exhibited the most promising antibacterial responses (see Section 3.6) – were treated at 700 °C and 750 °C for 3 h, in order to investigate which crystalline phases form following prolonged heat treatment. The treatment temperatures were chosen based on the DTA results, being not too far from the T_c or T_{c_onset} of the three glasses. The results are reported in Fig. 5.

The analysis reveals that the main crystalline phase formed is combeite ($Na_4Ca_4Si_6O_{18}$, JCPDS no. 01-079-1086). This is consistent with the crystallization behavior of 45S5 Bioglass®, in which combeite also forms as the primary crystalline phase, typically appearing above 600 °C [48]; additional crystalline phases may also form depending on the glass composition and the thermal treatment conditions [49]. Glass-ceramics containing crystalline phases may retain bioactivity, but the kinetics and uniformity of dissolution are altered. Crystallized 45S5 has been shown to remain bioactive, although it exhibits slower ion-release kinetics compared with the amorphous counterpart [50]. The relative proportions of the amorphous and crystalline fractions must be carefully considered and assessed when evaluating these glass-ceramics for biomedical applications [51].

3.4. In vitro bioactivity evaluation in SBF

Based on the antimicrobial results and considering that the main

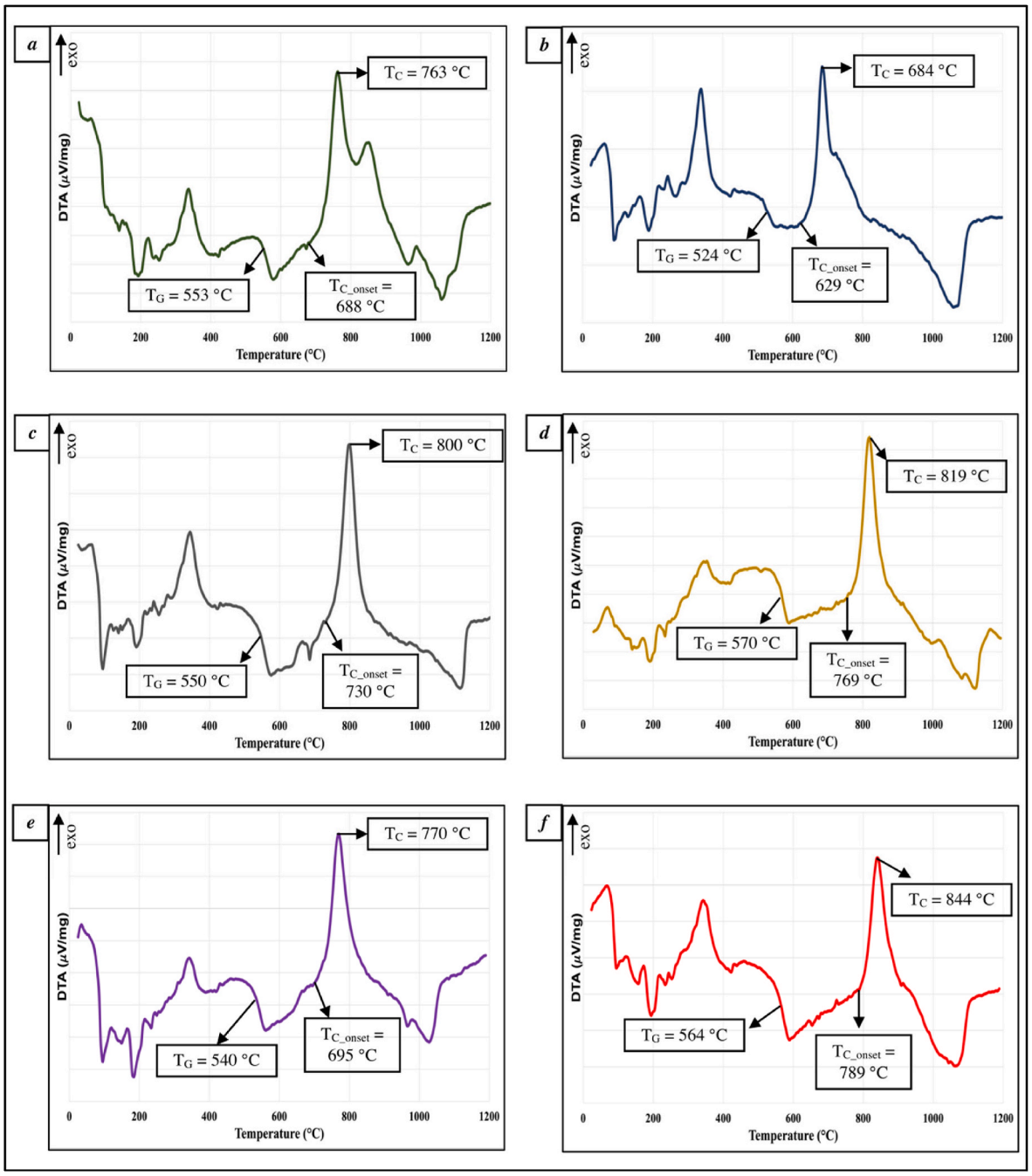

Fig. 3. DTA analysis of: a) Roma1, b) Roma2, c) Roma3, d) Roma4, e) Roma5, f) Roma6. The characteristic temperatures T_G, T_{C_onset} and T_C are shown on the curves.

objective of this study was to identify the BG composition with the most effective antibacterial properties against both Gram-positive and Gram-negative strains, subsequent experiments on bioactivity focused exclusively on the best-performing candidates: Roma1, Roma2, and Roma5.

Although in vitro SBF tests are relatively simple and have limitations, they provide a useful preliminary indication of a material's potential to bond with bone tissue *in vivo*. The principle of the test is based on immersing the sample in a solution that mimics the ionic composition of human blood plasma. In this context, bioactivity is assessed by examining the precipitation of HAp – analogous to the mineral phase of bone – on the surface of the biomaterial after immersion in SBF for various periods of time [52]. A crucial intermediate in the bioactivity mechanism of silicate-based BGs is the formation of hydrated silica gel [53], resulting from network dissolution and ion release. This porous, hydroxylated surface can act as a template for HAp nucleation. The negatively charged silanol groups (Si–OH) within this gel interact with Ca^{2+} and PO_4^{3-} ions from the surrounding medium, locally concentrating them and promoting the precipitation of calcium–phosphate species (Ca–P) that eventually crystallize into HAp [53]. Upon drying after SBF extraction, this silica-rich layer undergoes shrinkage and dehydration, producing the characteristic cracked morphology [53].

In vitro immersion tests in SBF of the three glass compositions showed a pronounced pH increase during each 48-h incubation period (Fig. 6). At each time point, after the SBF was refreshed, the pH returned to 7.4, and then gradually increased again over the next 48 h. Refreshing the fluid every 48 h is a commonly used procedure to roughly simulate the fluid turnover that would occur *in vivo* [54]. Roma2 consistently produced the highest change of pH (~8.6), followed by Roma1 (~8.4), and Roma5 showing the lowest pH excursion (~8.2). The cyclic increase reflects (i) rapid ion-exchange between the glass network (e.g. Na^+,

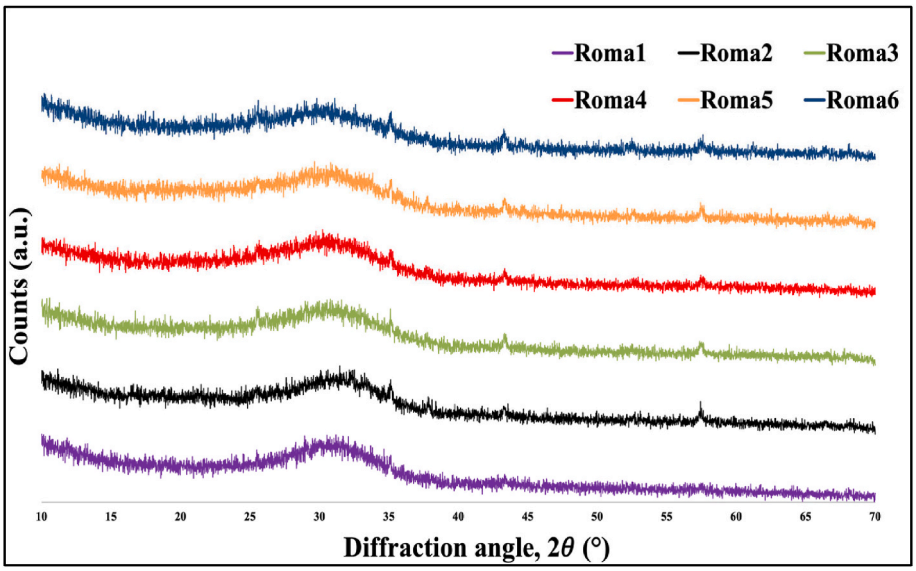

Fig. 4. XRD spectra of the as-produced BGs.

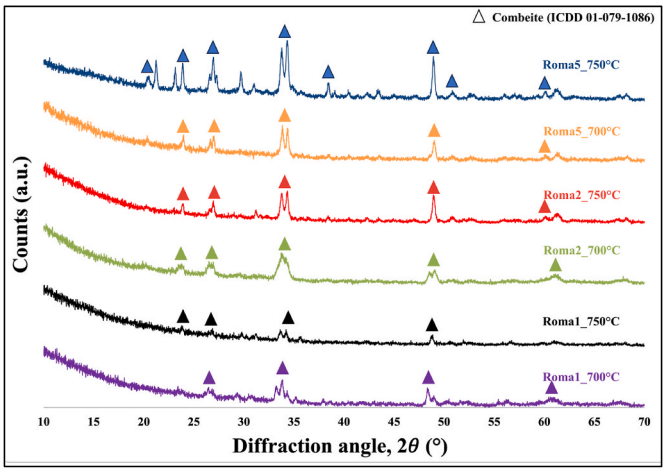

Fig. 5. XRD spectra of Roma1, Roma2, and Roma5 after heat treatment at 700 °C or 750 °C for 3 h.

Ca^{2+}, Mg^{2+}, Zn^{2+}) and the SBF protons (H^{+}), and (ii) subsequent partial dissolution of the silicate network, increasing the concentration of hydroxide ions (OH^{-}) in solution [55].

Overall, these data indicate that Roma2 has the most pronounced alkalizing effect in SBF, which may correlate with its antibacterial effectiveness (see section 3.6).

The morphology of the BG powders was examined by SEM before SBF immersion. Representative micrographs of Roma1, Roma2, and Roma5 are reported in Supplementary Fig. S1, showing no appreciable differences among the investigated compositions. As expected, the morphology of the powders was primarily governed by the common grinding and sieving procedure rather than by glass composition. Following 7 days of immersion in SBF, the sample surfaces were analyzed by SEM and their elemental composition was determined by EDX. The results are reported in Fig. 7 for representative samples: Roma1 (a), Roma2 (b), and Roma5 (c). The SEM micrographs show sparse spherical aggregates with a cauliflower-like morphology, which has frequently been associated with the early precipitation of calcium-phosphate phases during in vitro bioactivity tests [56]. These deposits are not homogeneously distributed but confined to isolated areas of the sample surface. This observation is consistent with the limited surface reactivity of the investigated compositions under the adopted test conditions. The fine and localized nature of the precipitates is further supported by XRD analysis of the samples after 7 days of immersion: the resulting spectra (reported in Fig. S2) closely resemble those of the as-prepared glasses (Fig. 4) and do not show diffraction peaks attributable to newly formed crystalline calcium-phosphate phases.

This behavior is consistent with previous studies showing that Zn-containing BGs generally exhibit reduced in vitro bioactivity compared with conventional bioactive glasses, primarily because Zn^{2+} and Mg^{2+} delay the nucleation and growth of hydroxyapatite. Both ions are reported to delay HAp formation during the early stages of immersion in SBF [43,57,58]. In particular: (i) Zn^{2+} can compete with Ca^{2+} at the glass–solution interface and form stable complexes with phosphate ions, thereby reducing the degree of supersaturation with respect to HAp [58]; and (ii) the substitution of Ca^{2+} with Mg^{2+}, which has a smaller ionic radius, increases the compactness of the glass network and the local oxygen density, leading to a reduced dissolution rate of the glass matrix [43]. Since the nucleation and growth rate of HAp is directly related to the supersaturation of the SBF, the lower Ca^{2+} availability and slower ion release caused by these substitutions result in delayed HAp precipitation. Therefore, the limited surface reactivity observed in these BG compositions during the first 7 days of SBF immersion is consistent with the presence of Zn^{2+} and Mg^{2+} in the glass network. However, the incorporation of these ions was not primarily intended to enhance the in vitro bioactivity of the glasses, but rather to combine the biological benefits of magnesium with the antibacterial properties of zinc, while simultaneously investigating their influence on the characteristic temperatures of the glasses and their tendency to crystallize upon heat treatment.

The EDX spectra (Fig. 8a and b) provide further insight into the surface reactions. A pronounced silicon signal is consistently detected, suggesting the likely formation of a silica-rich layer at the glass–SBF interface. Moreover, the EDX analysis shows an increase in phosphorus content compared with the original BG, indicating the accumulation of calcium- and phosphorus-rich surface deposits. The semi-quantitative EDX analysis further indicates that the Ca/P ratios of these deposits deviate from the stoichiometric value of hydroxyapatite (Ca/P = 1.67). Together with the absence of diffraction peaks attributable to HAp in the XRD patterns after 7 days of immersion (Fig. S2), this suggests that the observed deposits may correspond to non-stoichiometric calcium-phosphate-rich precipitates, possibly related to amorphous calcium phosphate (ACP)-like precursor phases, rather than crystalline HAp.

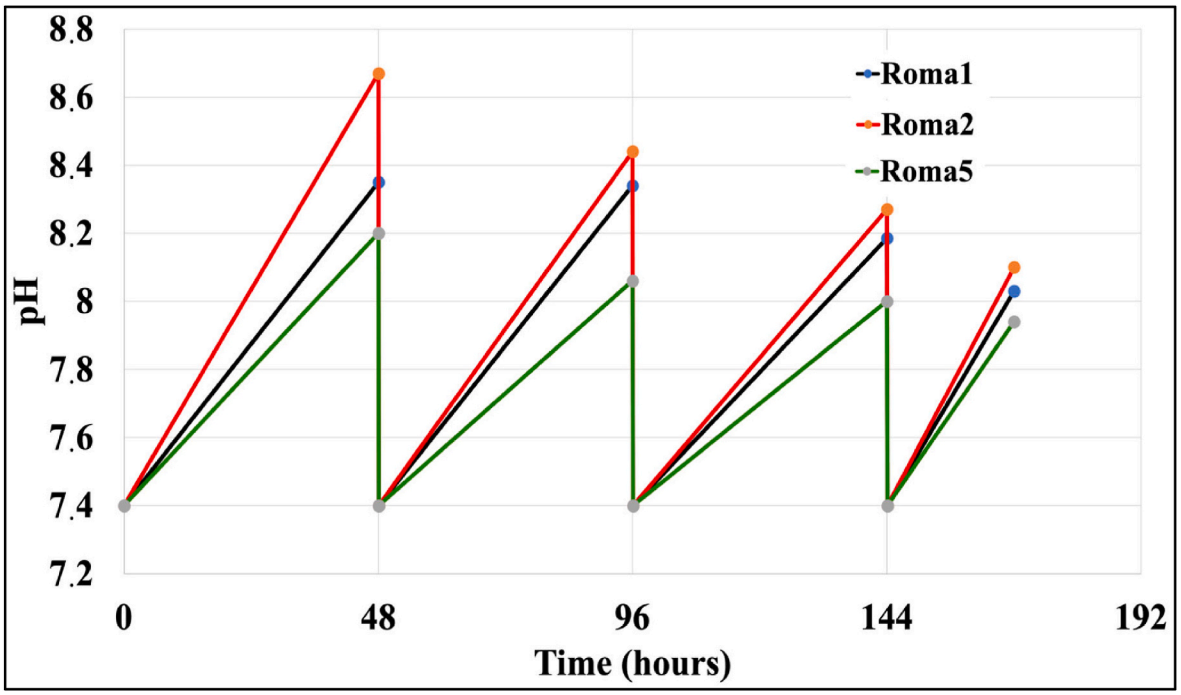

Fig. 6. pH variation induced by the samples in SBF.

These findings are consistent with the initial stages of the well-established bioactivity mechanism of silicate-based BGs, involving silica gel formation and the precipitation of calcium-phosphate-rich surface layers.

3.5. Measurement of ion release

Figs. 9–14 (a-c) present the results of ion release measurements performed on Roma1, Roma2, and Roma5 samples, analyzed by ICPMS/TQ. The experiments were carried out in Milli-Q water (blank) over immersion periods of 1, 3, and 7 days. Ion concentrations, expressed in parts per million (ppm), are shown relative to the corresponding values in the blank solution. The limited variation shown by the error bars reflects good reproducibility of the measurements.

Looking more closely at the ion release trends, the data reveal distinct release behaviors among the different ions:

(i) calcium (Ca^{2+}) showed an increasing release into solution for all samples except Roma2. In this case, the lower Ca^{2+} concentration may be linked to its incorporation into Ca–P surface layers, reducing its availability in the medium;
(ii) magnesium (Mg^{2+}) concentrations tended to decrease with time, suggesting that part of the released Mg^{2+} may reprecipitate on the glass surface;
(iii) sodium (Na^{+}) generally exhibited an increasing release profile in all samples (except for a slight decrease after 3 days in Roma2);
(iv) phosphorus release, extracted in the solution as phosphate ions (PO_4^{3-}), also decreased over time, supporting the hypothesis of precipitation processes involving calcium-phosphate phases;
(v) silicon (Si^{4+}), the primary glass network former, consistently increased throughout the test period, indicating depolymerization of the glass network;
(vi) zinc (Zn^{2+}) release increased over time for Roma1 and Roma2, while the trend is less clear for Roma5.

Among the detected ions, Zn^{2+} release is probably one of the main contributors to the antibacterial properties of these BGs. Together with the alkalinization observed during the SBF tests, Zn^{2+} release is expected to contribute significantly to the antimicrobial performance of the investigated compositions [59]. However, the release of other ions may also contribute to the observed antimicrobial activity. In particular, Mg^{2+} may exert an antibacterial effect by slightly increasing the local pH and influencing the membrane stability of bacteria [60,61]. Similarly, the release of Na^{+} and Si^{4+} – both showing an increasing release over time in most cases – may contribute to antibacterial effects, with Na^{+} creating a less favorable environment for microbial growth through osmotic and pH changes, and Si^{4+} possibly influencing bacterial metabolism and adhesion indirectly [62]. Although these contributions are less pronounced than that of Zn^{2+}, they may act synergistically, enhancing the overall antibacterial performance of the produced BGs. It should be noted that the present ion-release measurements were performed in Milli-Q water to evaluate the intrinsic dissolution behavior of the investigated glasses under controlled conditions. Consequently, the measured concentrations should not be considered directly representative of ion release under physiological conditions, where the presence of dissolved ions, proteins, and precipitation phenomena may significantly influence dissolution kinetics. Accordingly, the present results should primarily be interpreted as a comparative assessment of the intrinsic dissolution behavior of the investigated formulations rather than as a direct prediction of the *in vivo* ion-release profile of the investigated glasses. Future work will therefore investigate ion release in physiologically relevant media, such as SBF and DMEM, to evaluate whether the comparative dissolution trends observed under simplified conditions are maintained under conditions more closely resembling the physiological environment.

3.6. Antibacterial properties

The antimicrobial performance of the tested BGs varied markedly across both materials and bacterial species (see Figs. 15 and 16). Against *Escherichia coli*, Roma2 and Roma5 exhibited the highest efficacy, achieving nearly complete growth inhibition. Roma1 and Roma3 showed intermediate activity, reducing bacterial proliferation by approximately 80%, whereas Roma4 displayed the weakest effect, limiting growth by about 60%. Roma6 performed slightly better than Roma4 but did not reach the inhibitory levels of the top-performing

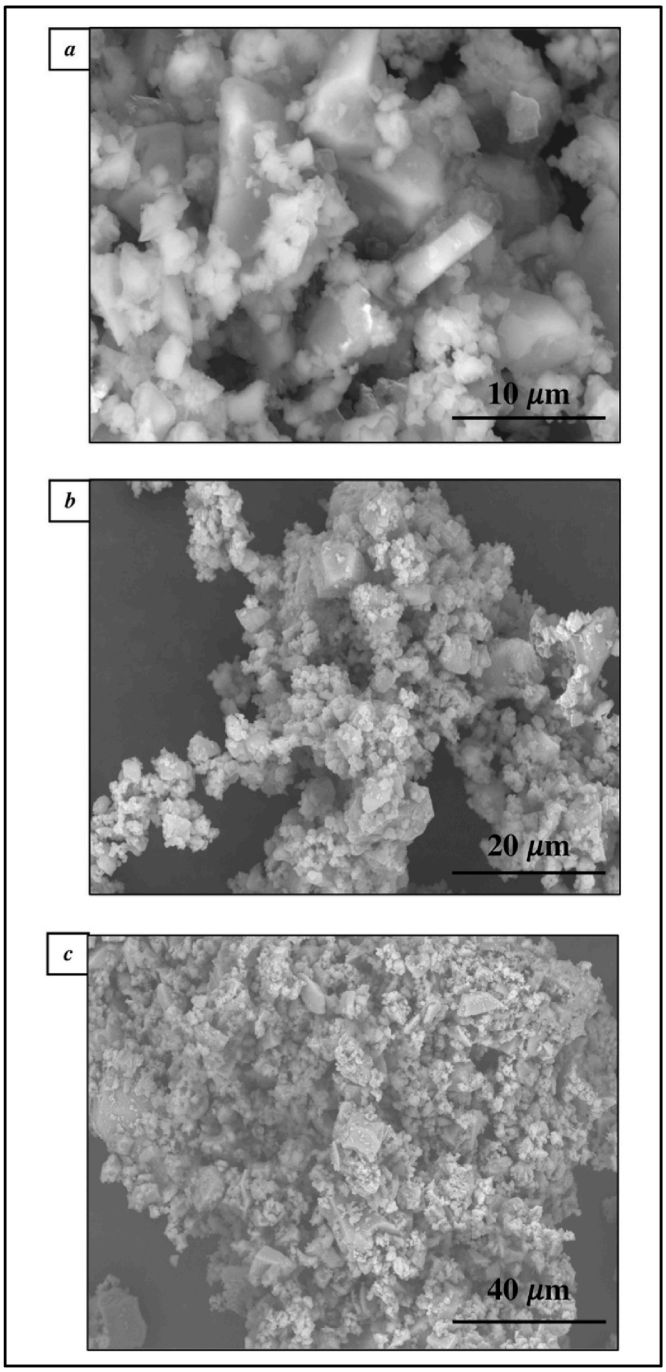

Fig. 7. SEM-FEG micrographs of samples after 7 days of soaking in SBF: (a) Roma1; (b) Roma2; (c) Roma5.

formulations. The variability among replicates, reflected in the error bars, suggests that intrinsic physicochemical features of the BGs – such as particle size, surface charge, or interactions with the bacterial envelope – likely account for their distinct activities.

Comparable differences were observed against *Staphylococcus aureus*. Roma2 again emerged as the most effective, almost completely suppressing bacterial growth. Roma1, Roma5, and Roma6 produced moderate inhibition (65%–75%), while Roma3 and Roma4 showed lower suppression levels (50%–60%). The reproducible variation among formulations highlights that even small structural or compositional differences can strongly influence antimicrobial potency. Overall, these findings indicate that the tested BGs exhibit formulation-dependent and species-specific antibacterial effects. The superior and consistent efficacy of Roma2 against both Gram-negative and Gram-positive bacteria suggests that this formulation possesses optimal physicochemical characteristics for antimicrobial performance [63].

The antibacterial trends observed in the present study are generally consistent with previous investigations reporting enhanced antimicrobial activity in Zn-containing bioactive glasses, particularly against *E. coli* and *S. aureus* [7,8,11,52]. Increasing Zn content has been shown to improve the antibacterial efficacy of both melt-derived and sol-gel-derived BGs against Gram-positive and Gram-negative bacteria [64–66].

However, the antibacterial activity of the investigated Zn/Mg-containing BGs should be interpreted as the result of multiple concurrent mechanisms rather than as the effect of a single released species. Upon contact with the aqueous medium, BG dissolution promotes ion exchange and the release of soluble ionic species, including Zn^{2+}, Na^{+}, Mg^{2+} and silicate species, together with an increase in medium pH. Such alkalinization may disturb bacterial homeostasis, alter membrane transport, and create an unfavorable environment for bacterial proliferation. This interpretation is consistent with the general design principles of antimicrobial biomaterials, for which recent literature emphasizes that efficient antibacterial performance often relies on the combination of multiple mechanisms, including active bactericidal action, modulation of bacterial adhesion, and interference with biofilm development [10,17]. In parallel, Zn^{2+} release is expected to play a major role because zinc-containing materials have been reported to exhibit broad-spectrum antibacterial effects against both Gram-negative and Gram-positive bacteria, including *E. coli* and *S. aureus* [10,17]. Zn^{2+} can interfere with bacterial metal homeostasis, promote oxidative stress through reactive oxygen species generation, and impair membrane and intracellular functions.

The higher and more consistent antibacterial efficacy of Roma2 against both bacterial strains can therefore be tentatively attributed to the combined effect of sustained Zn^{2+} release and stronger medium alkalinization. However, the contribution of other ions should not be neglected. Na^{+} release may contribute to osmotic and pH-related stress, while Mg^{2+} and soluble silicate species may indirectly affect bacterial membrane stability, adhesion, and metabolism. The different responses observed for *E. coli* and *S. aureus* may also reflect their distinct cell-envelope architectures, with the outer membrane of Gram-negative bacteria and the thicker peptidoglycan layer of Gram-positive bacteria modulating their susceptibility to ionic and alkaline stress. Since the present assay was based on BG-derived eluates, soluble ion release and pH variation are likely the dominant mechanisms, whereas direct particle–bacteria contact effects should not be considered, since there were no residual particles present in the eluates.

Moreover, other factors can contribute to the observed differences in antimicrobial activity, and further studies are warranted to clarify the underlying mechanisms, besides the Zn content, including particle–cell wall interactions, penetration efficiency, and stability under physiological conditions. One of these factors is the dissolution behavior of the BG, which depends on its composition. Although directly correlating the dissolution behavior of a BG with the specific content of network-forming and network-modifying ions is challenging, useful insights can be obtained from calculating the network connectivity (NC), which reflects the degree of polymerization of the silicate network and can help predict the glass's reactivity and ion-release profile. The NC, which represents the average number of bridging oxygen atoms per silicon atom, is widely used in the literature as an indicator of how a BG's oxide composition affects its reactivity and bioactivity [67,68]. Following Blochberger et al. [32] and Brauer [69], Table 3 reports NC values calculated assuming that Mg and Zn behave as typical network modifiers, using the formula proposed by Hill and Brauer (2011) [67], and later discussed by Jones (2015) [68]:

$$NC = \frac{4[SiO_2] - 2\left[M^{I}_{2}O + M^{II}O\right] + 6[P_2O_5]}{[SiO_2]}$$

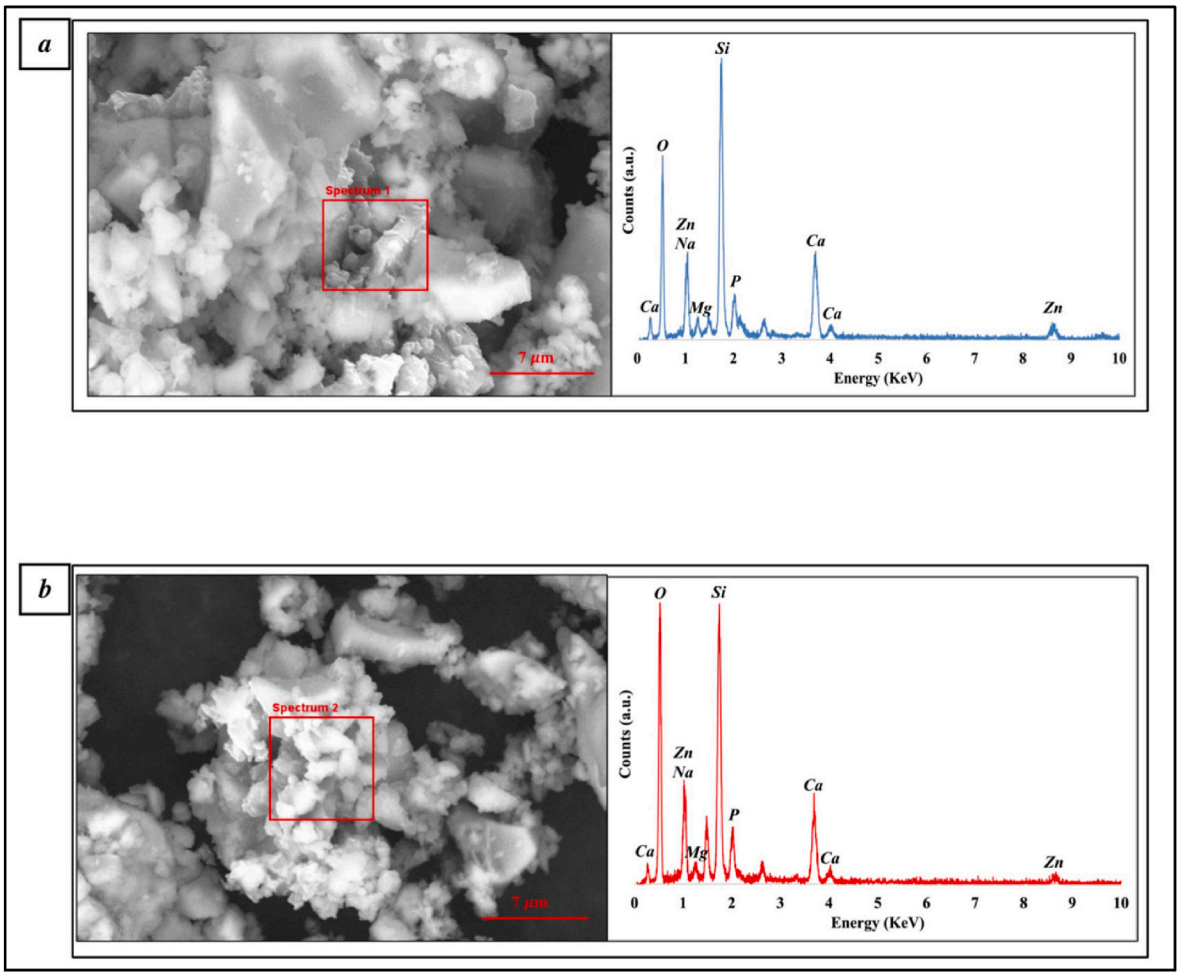

Fig. 8. (a) SEM-FEG micrograph of Roma1 sample after 7 days of soaking in SBF, with EDX analysis of the highlighted (red) area. (b) SEM-FEG micrograph of Roma2 sample after 7 days of soaking in SBF, and EDX analysis of the highlighted (red) area.

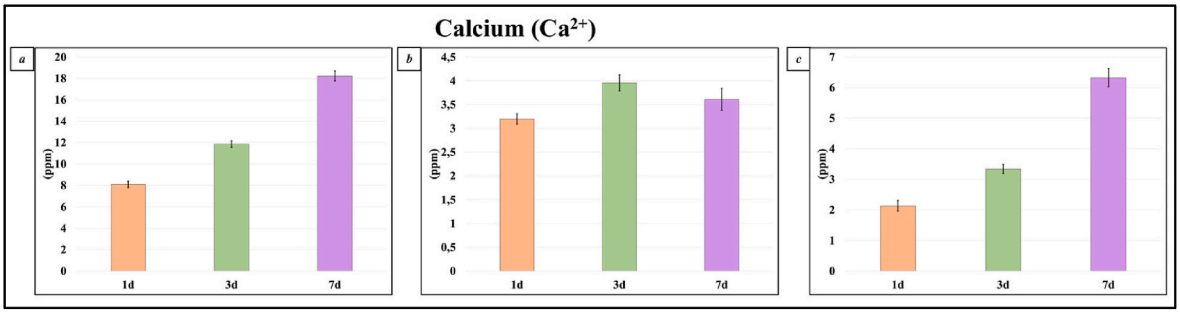

Fig. 9. Calcium ion concentrations measured by ICP-MS/TQ in Milli-Q water (blank) for (a) Roma1, (b) Roma2, and (c) Roma5. Orange, green, and purple bars represent ion release after 1, 3, and 7 days of immersion, respectively.

where $M^{II}O$ and $M^{I}_{2}O$ are the mono- and divalent modifier oxides in the glass. This approach is widely adopted in the literature for comparative purposes, although it represents a simplified description of the glass structure, since Zn may also act as an intermediate species depending on its local coordination environment and the overall glass composition.

The NC obtained for these BGs confirms the values commonly reported in the literature [13,14,32,43,69], supporting the adopted structural interpretation within the limitations of the NC model. As extensively highlighted by Brauer [69], BGs with a higher degree of cross-linking – typically those with NC values above 2.4 – tend to exhibit reduced dissolution and ion release due to their more polymerized network. Conversely, lower NC values indicate increased network depolymerization and therefore faster dissolution kinetics, which can enhance the release of biologically relevant ions contributing to antibacterial action [67,68]. Importantly, the substitution of different modifier cations can significantly influence physical properties such as density, hardness, or T_C, even when NC remains constant [69].

In this study, NC provides a useful qualitative framework for interpreting the antimicrobial trends. Roma1 and Roma2 have the same NC (2.20), which is lower than that of Roma5 (2.53). Lower NC values (e.g., Roma1 and Roma2 compared with Roma5) indicate a less cross-linked network, a higher susceptibility to hydrolysis and a more rapid release

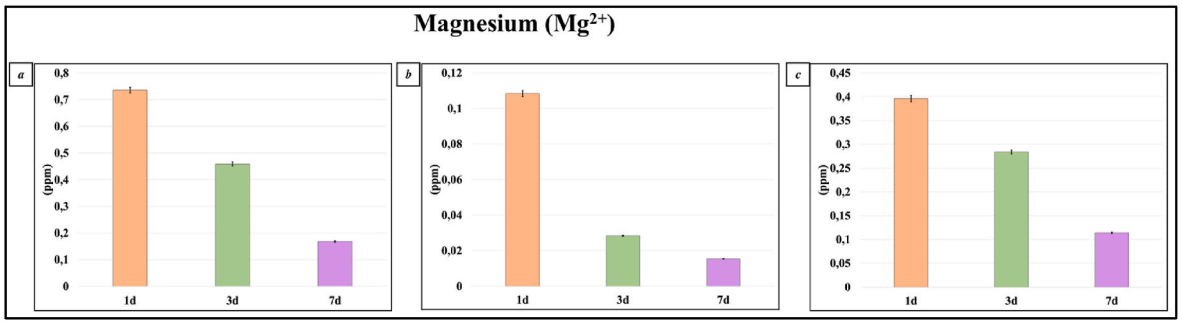

Fig. 10. Magnesium ion concentrations measured by ICP-MS/TQ in Milli-Q water (blank) for (a) Roma1, (b) Roma2, and (c) Roma5. Orange, green, and purple bars represent ion release after 1, 3, and 7 days of immersion, respectively.

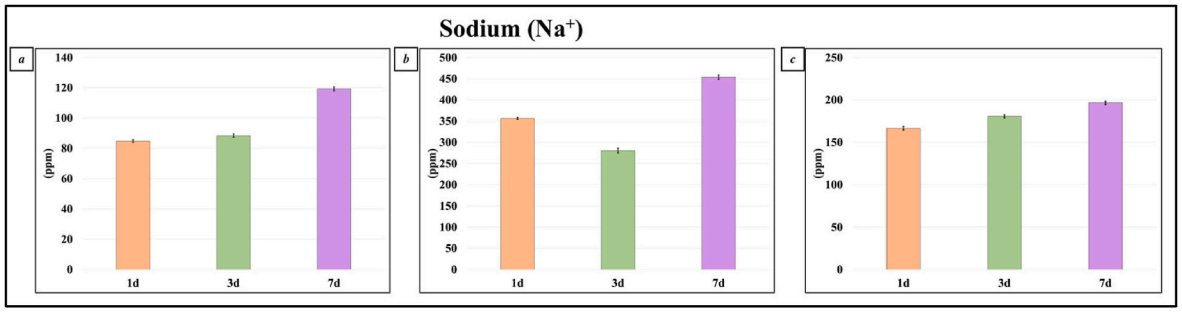

Fig. 11. Sodium ion concentrations measured by ICP-MS/TQ in Milli-Q water (blank) for (a) Roma1, (b) Roma2, and (c) Roma5. Orange, green, and purple bars represent ion release after 1, 3, and 7 days of immersion, respectively.

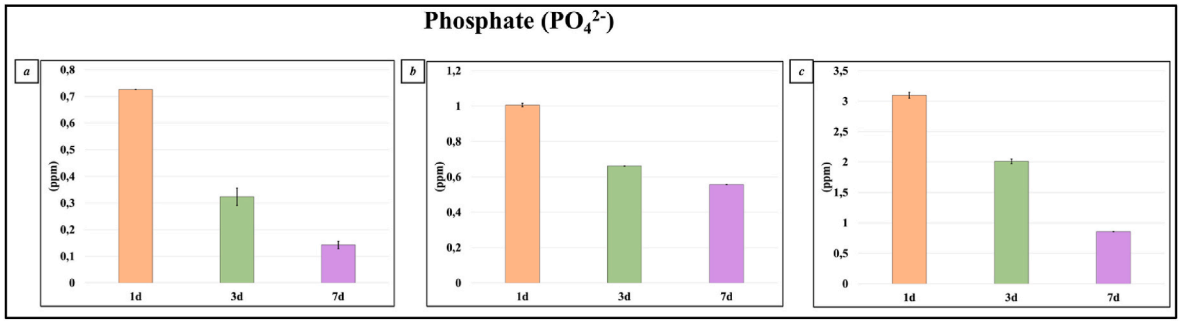

Fig. 12. Phosphate ion concentrations measured by ICP-MS/TQ in Milli-Q water (blank) for (a) Roma1, (b) Roma2, and (c) Roma5. Orange, green, and purple bars represent ion release after 1, 3, and 7 days of immersion, respectively.

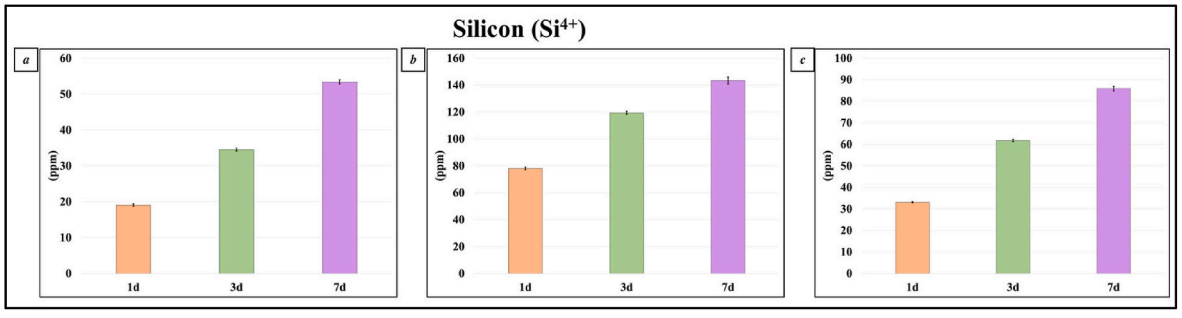

Fig. 13. Silicon ion concentrations measured by ICP-MS/TQ in Milli-Q water (blank) for (a) Roma1, (b) Roma2, and (c) Roma5. Orange, green, and purple bars represent ion release after 1, 3, and 7 days of immersion, respectively.

of soluble ionic species, promoting stronger antibacterial effects; at the same time, Roma2 contains and releases more zinc than Roma1 (see Fig. 14). Therefore, the superior antibacterial performance of Roma2 is likely to result from the combined effects of multiple factors, such as glass network connectivity, Zn release coupled with the contribution of other ions, and other compositional factors, rather than from NC alone.

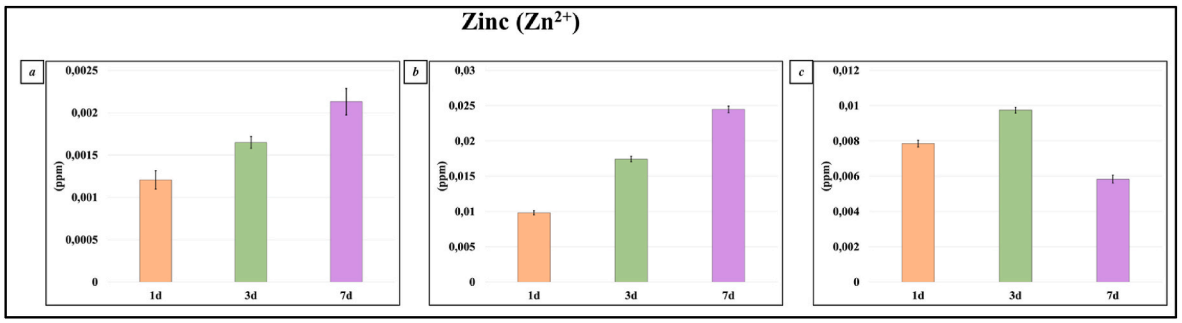

Fig. 14. Zinc ion concentrations measured by ICP-MS/TQ in Milli-Q water (blank) for (a) Roma1, (b) Roma2, and (c) Roma5. Orange, green, and purple bars represent ion release after 1, 3, and 7 days of immersion, respectively.

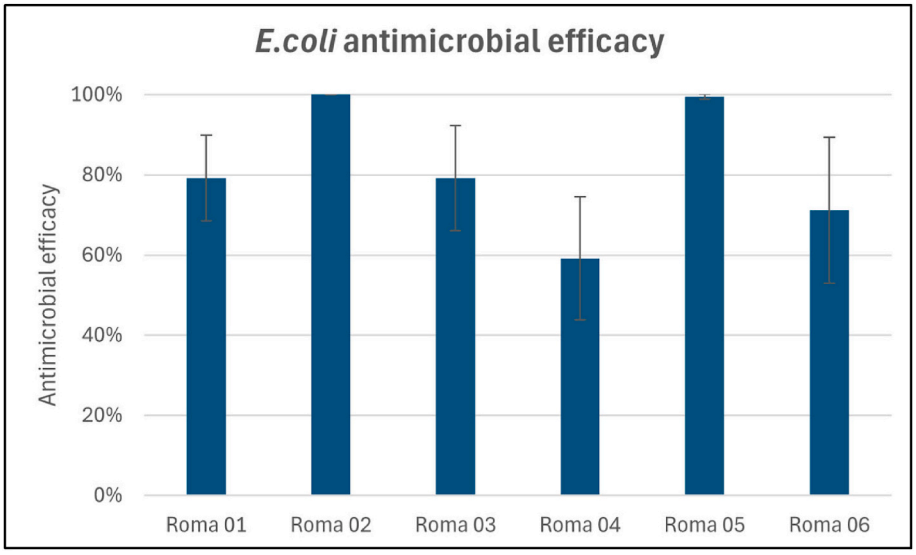

Fig. 15. Antimicrobial efficacy of the produced BGs against *E. coli*. Efficacy was expressed as the percentage reduction in colony-forming units (CFUs) relative to untreated controls. Error bars denote standard deviations from duplicate experiments.

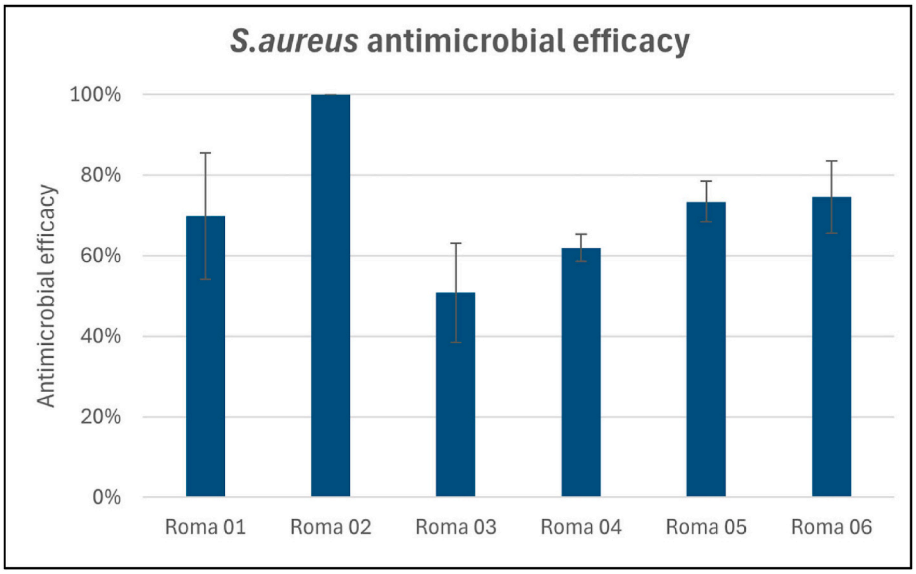

Fig. 16. Antimicrobial efficacy of the produced BGs against *S. aureus*. Efficacy was expressed as the percentage reduction in CFUs relative to untreated controls. Error bars denote standard deviations from duplicate experiments.

Table 3
– Network connectivity (NC) calculated assuming Zn/Mg to act as network modifiers and compared with the NC of 45S5 Bioglass® and S53P4 [69].

Sample	*Roma1*	*Roma2*	*Roma3*	*Roma4*	*Roma5*	*Roma6*	45S5 Bioglass®	*S53P4*
NC	2.20	2.20	2.20	2.20	2.53	2.53	2.12	2.54

4. Conclusions

The present study highlights how variations in composition can significantly influence the structural, physicochemical, and biological performance of Zn/Mg-containing BGs. The compositional complexity, incorporating multiple ionic species, makes it challenging to disentangle the individual effects of each ion on the material's properties. The same ionic species may exhibit markedly different behavior depending on their local coordination environment, concentration, and synergistic interactions with other ions. Compositions with lower Na_2O content, or in which Zn acted predominantly as a network former, displayed reduced reactivity and weaker antimicrobial effects. Overall, the Roma2 formulation represents an optimal balance, with Zn functioning as a network modifier that enhances structural stability while ensuring high reactivity and sustained Zn release, under the adopted experimental conditions. These combined properties support its superior antimicrobial performance, identifying Roma2 as the most promising candidate among the tested formulations for future biomedical applications.

CRediT authorship contribution statement

D. Bellucci: Writing – review & editing, Writing – original draft, Investigation. **F. Basoli:** Writing – review & editing, Writing – original draft, Investigation, Funding acquisition. **S. De Micco:** Writing – original draft, Investigation. **E. D'Alessandro:** Writing – original draft, Investigation. **S. Grasso:** Writing – original draft, Investigation. **M. Giovanetti:** Writing – original draft, Investigation. **M. Trombetta:** Writing – review & editing, Supervision, Methodology. **V. Cannillo:** Writing – review & editing, Supervision, Methodology, Funding acquisition, Conceptualization.

Declaration of competing interest

The authors declare that they have no known competing financial interests or personal relationships that could have appeared to influence the work reported in this paper.

Acknowledgments

Funding for this research was provided under the National Recovery and Resilience Plan (NRRP), Mission 4, Component 2, Investment 1.1, Call for tender No. 1409 published on 14.9.2022 by the Italian Ministry of University and Research (MUR), funded by the European Union – NextGenerationEU– Project Title GAiA - Zero Waste Green Made Antimicrobial Filtering Face Piece Fibers for Augmented Individual Protection – CUP C53D23008340001- Grant Assignment Decree No. 966 adopted on 30/06/2023 by the Italian Ministry of University and Research (MUR). Devis Bellucci and Valeria Cannillo wish to thank Dr. Francesco Gerardo Mecca and Dr. Andrea Martelli for their assistance during the in vitro tests in SBF, and Dr. Daniela Manzini for her help with the ionic release measurements performed using ICP-MS TQ.

Appendix A. Supplementary data

Supplementary data to this article can be found online at https://doi.org/10.1016/j.matchemphys.2026.132958.

Data availability

Data will be made available on request.

References

[1] L.L. Hench, The story of bioglass®, J. Mater. Sci. Mater. Med. (2006) 967–978, https://doi.org/10.1007/s10856-006-0432-z.
[2] E. Piatti, M. Miola, E. Verné, Tailoring of bioactive glass and glass-ceramics properties for in vitro and in vivo response optimization: a review, Biomater. Sci. 12 (2024) 4546–4589, https://doi.org/10.1039/d3bm01574b.
[3] M.H. Kaou, M. Furkó, K. Balázsi, C. Balázsi, Advanced bioactive glasses: the newest achievements and breakthroughs in the area, Nanomaterials 13 (2023), https://doi.org/10.3390/nano13162287.
[4] F.G. Mecca, D. Bellucci, V. Cannillo, Effect of thermal treatments and ion substitution on sintering and crystallization of bioactive glasses: a review, Materials 16 (2023), https://doi.org/10.3390/ma16134651.
[5] M. Godoy-Gallardo, U. Eckhard, L.M. Delgado, Y.J.D. de Roo Puente, M. Hoyos-Nogués, F.J. Gil, R.A. Perez, Antibacterial approaches in tissue engineering using metal ions and nanoparticles: from mechanisms to applications, Bioact. Mater. 6 (2021) 4470–4490, https://doi.org/10.1016/j.bioactmat.2021.04.033.
[6] M.S. Shoushtari, D. Hoey, D.R.A. Biak, N. Abdullah, S. Kamarudin, H.S. Zainuddin, Sol–gel-templated bioactive glass scaffold: a review, Res. Biomed. Eng. 40 (2024) 281–296, https://doi.org/10.1007/s42600-024-00342-x.
[7] L. Drago, M. Toscano, M. Bottagisio, Recent evidence on bioactive glass antimicrobial and antibiofilm activity: a mini-review, Materials 11 (2018), https://doi.org/10.3390/ma11020326.
[8] S. Begum, W.E. Johnson, T. Worthington, R.A. Martin, The influence of pH and fluid dynamics on the antibacterial efficacy of 45S5 bioglass, Biomed. Mater. 11 (2016), https://doi.org/10.1088/1748-6041/11/1/015006.
[9] L. Hupa, N.C. Lindfors, Bioactive glass S53P4-from a statistically suggested composition to clinical success, in: Bioactive Glasses and Glass-Ceramics: Fundamentals and Applications, wiley, 2022, pp. 17–31, https://doi.org/10.1002/9781119724193.ch3.
[10] R. Zhang, H. Lin, Z. Wang, S. Cheng, C. Li, Y. Wang, Research progress on antimicrobial biomaterials, Macromol. Biosci. 25 (2025), https://doi.org/10.1002/mabi.202500239.
[11] F.G. Mecca, D. Bellucci, V. Cannillo, Bioactive glasses as antibacterial agents: a review, Int. J. Appl. Ceram. Technol. 23 (2026), https://doi.org/10.1111/ijac.70242.
[12] F. Sharifianjazi, M. Sharifianjazi, M. Irandoost, K. Tavamaishvili, M. Mohabatkhah, M. Montazerian, Advances in zinc-containing bioactive glasses: a comprehensive review, J. Funct. Biomater. 15 (2024), https://doi.org/10.3390/jfb15090258.
[13] I. Cacciotti, Bivalent cationic ions doped bioactive glasses: the influence of magnesium, zinc, strontium and copper on the physical and biological properties, J. Mater. Sci. 52 (2017) 8812–8831, https://doi.org/10.1007/s10853-017-1010-0.
[14] A. Goel, S. Kapoor, A. Tilocca, R.R. Rajagopal, J.M.F. Ferreira, Structural role of zinc in biodegradation of alkali-free bioactive glasses, J. Mater. Chem. B 1 (2013) 3073–3082, https://doi.org/10.1039/c3tb20163e.
[15] M. Prabhu, K. Kavitha, P. Manivasakan, V. Rajendran, P. Kulandaivelu, Synthesis, characterization and biological response of magnesium- substituted nanobioactive glass particles for biomedical applications, Ceram. Int. 39 (2013) 1683–1694, https://doi.org/10.1016/j.ceramint.2012.08.011.
[16] P.A. Dash, S. Mohanty, S.K. Nayak, Synthesis and characterization of ZnO/MgO doped mesoporous bioactive glass: enhanced bioactivity and antibacterial properties for bone tissue engineering applications, Ceram. Int. 51 (2025) 38129–38140, https://doi.org/10.1016/j.ceramint.2025.06.049.
[17] Y. Xie, C. Dong, Z. Liu, Y. Yi, Y. Zhou, The influence of rolling reduction on the mechanical, corrosion, osteogenic, and antibacterial properties of Zn–Mg alloys, ACS Omega 10 (2025) 37141–37153, https://doi.org/10.1021/acsomega.5c01732.
[18] T. Tsuruoka, A. Kodama, S. Yamaguchi, T. Masutomi, A. Koyama, T. Murohara, K. Komori, R. Shibata, Zinc deficiency impairs ischemia-induced angiogenesis, JVS. Vasc. Sci. 3 (2022) 30–40, https://doi.org/10.1016/j.jvssci.2021.09.023.
[19] F. Rehder, M. Arango-Ospina, S. Decker, M. Saur, E. Kunisch, A. Moghaddam, T. Renkawitz, A.R. Boccaccini, F. Westhauser, The addition of zinc to the ICIE16-Bioactive glass composition enhances osteogenic differentiation and matrix formation of human bone marrow-derived mesenchymal stromal cells, Biomimetics 9 (2024), https://doi.org/10.3390/biomimetics9010053.
[20] C.R. Mendes, G. Dilarri, C.F. Forsan, V. de M.R. Sapata, P.R.M. Lopes, P.B. de Moraes, R.N. Montagnolli, H. Ferreira, E.D. Bidoia, Antibacterial action and target mechanisms of zinc oxide nanoparticles against bacterial pathogens, Sci. Rep. 12 (2022), https://doi.org/10.1038/s41598-022-06657-y.
[21] N. Pangprasit, A. Kongkaew, D. Saipinta, S. Pikulkaew, M. Intanon, W. Suriyasathaporn, W. Chaisri, Evaluation of antibacterial properties of zinc oxide nanoparticles against bacteria isolated from animal wounds, Pharmaceutics 17 (2025), https://doi.org/10.3390/pharmaceutics17020209.
[22] T.-N. Phan, T. Buckner, J. Sheng, J.D. Baldeck, R.E. Marquis, Physiologic actions of zinc related to inhibition of acid and alkali production by oral streptococci in suspensions and biofilms, Oral Microbiol. Immunol. 19 (2004) 31–38.
[23] D. Bellucci, A. Mazzilli, A. Martelli, F.G. Mecca, S. Bonacorsi, F.D. Lofaro, F. Boraldi, D. Quaglino, V. Cannillo, Enrichment of strontium and magnesium

improves the physical, mechanical and biological properties of bioactive glasses undergoing thermal treatments: new cues for biomedical applications, Ceram. Int. 50 (2024) 52819–52837, https://doi.org/10.1016/j.ceramint.2024.10.135.
[24] V.K.H. Bui, D. Park, Y.C. Lee, Chitosan combined with ZnO, TiO2 and Ag nanoparticles for antimicrobialwound healing applications: a mini review of the research trends, Polymers (Basel) 9 (2017), https://doi.org/10.3390/polym9010021.
[25] V. Anand, K.J. Singh, K. Kaur, Evaluation of zinc and magnesium doped 45S5 mesoporous bioactive glass system for the growth of hydroxyl apatite layer, J. Non. Cryst. Solids 406 (2014) 88–94, https://doi.org/10.1016/j.jnoncrysol.2014.09.050.
[26] M.M. Almoudi, A.S. Hussein, M.I. Abu Hassan, N. Mohamad Zain, A systematic review on antibacterial activity of zinc against Streptococcus mutans, Saudi Dent. J. 30 (2018) 283–291, https://doi.org/10.1016/j.sdentj.2018.06.003.
[27] N. Kanzaki, K. Onuma, G. Treboux, S. Tsutsumi, A. Ito, Inhibitory effect of magnesium and zinc on crystallization kinetics of hydroxyapatite (0001) face, J. Phys. Chem. B 104 (2000) 4189–4194, https://doi.org/10.1021/jp9939726.
[28] P. Balasubramanian, L.A. Strobel, U. Kneser, A.R. Boccaccini, Zinc-containing bioactive glasses for bone regeneration, dental and orthopedic applications, Biomed. Glass. 1 (2015) 51–69, https://doi.org/10.1515/bglass-2015-0006.
[29] A.I. Damian-Buda, C.D. Ghiţulică, A. Cucuruz, G. Voicu, D. Culita, V. Fruth-Oprişan, L.T. Ciocan, Mesoporous bioactive glass nanoparticles in the SiO2-P2O5-CaO-MO (M=Mg, Zn) system: synthesis and properties, J, Funct. Biomater. 13 (2022), https://doi.org/10.3390/jfb13040180.
[30] R. Wetzel, O. Bartzok, D.S. Brauer, Influence of low amounts of zinc or magnesium substitution on ion release and apatite formation of bioglass 45S5, J. Mater. Sci. Mater. Med. 31 (2020), https://doi.org/10.1007/s10856-020-06426-1.
[31] Z. Tabia, K. El Mabrouk, M. Bricha, K. Nouneh, Mesoporous bioactive glass nanoparticles doped with magnesium: drug delivery and acellular: in vitro bioactivity, RSC Adv. 9 (2019) 12232–12246, https://doi.org/10.1039/c9ra01133a.
[32] M. Blochberger, L. Hupa, D.S. Brauer, Influence of zinc and magnesium substitution on ion release from bioglass 45S5 at physiological and acidic pH, Biomedical Glasses 1 (2015) 93–107, https://doi.org/10.1515/bglass-2015-0009.
[33] O. Bretcanu, X. Chatzistavrou, K. Paraskevopoulos, R. Conradt, I. Thompson, A. R. Boccaccini, Sintering and crystallisation of 45S5 bioglass® powder, J. Eur. Ceram. Soc. 29 (2009) 3299–3306, https://doi.org/10.1016/j.jeurceramsoc.2009.06.035.
[34] H. Jabraoui, Y. Vaills, A. Hasnaoui, M. Badawi, S. Ouaskit, Effect of sodium oxide modifier on structural and elastic properties of silicate glass, J. Phys. Chem. B 120 (2016) 13193–13205, https://doi.org/10.1021/acs.jpcb.6b09664.
[35] D. Bellucci, V. Cannillo, Low-temperature sintering of a new bioactive glass enriched with magnesium oxide and strontium oxide, Materials 15 (2022), https://doi.org/10.3390/ma15186263.
[36] T. Kokubo, H. Takadama, How useful is SBF in predicting in vivo bone bioactivity? Biomaterials 27 (2006) 2907–2915, https://doi.org/10.1016/j.biomaterials.2006.01.017.
[37] J.R. Jones, P. Sepulveda, L.L. Hench, Dose-dependent behavior of bioactive glass dissolution, J. Biomed. Mater. Res. 58 (2001) 720–726, https://doi.org/10.1002/jbm10053.
[38] A.M. George, J.F. Stebbins, Structure and Dynamics of Magnesium in Silicate Melts: a high-temperature 25 Mg NMR Study, 1998.
[39] K. Shimoda, Y. Tobu, M. Hatakeyama, T. Nemoto, K. Saito, Structural investigation of Mg local environments in silicate glasses by ultra-high field 25Mg 3QMAS NMR spectroscopy, Am. Mineral. 92 (2007) 695–698, https://doi.org/10.2138/am.2007.2535.
[40] R. Wetzel, M. Blochberger, F. Scheffler, L. Hupa, D.S. Brauer, Mg or Zn for Ca substitution improves the sintering of bioglass 45S5, Sci. Rep. 10 (2020), https://doi.org/10.1038/s41598-020-72091-7.
[41] G.S. Lázaro, S.C. Santos, C.X. Resende, E.A. Dos Santos, Individual and combined effects of the elements Zn, Mg and Sr on the surface reactivity of a SiO2·CaO·Na 2O·P2O5 bioglass system, J. Non. Cryst. Solids 386 (2014) 19–28, https://doi.org/10.1016/j.jnoncrysol.2013.11.038.
[42] R. Wetzel, O. Bartzok, L. Hupa, D.S. Brauer, Low Mg or Zn substitution for improved thermal properties of bioglass 45S5, Mater. Lett. 256 (2019), https://doi.org/10.1016/j.matlet.2019.126599.
[43] S.J. Watts, R.G. Hill, M.D. O'Donnell, R.V. Law, Influence of magnesia on the structure and properties of bioactive glasses, J. Non. Cryst. Solids 356 (2010) 517–524, https://doi.org/10.1016/j.jnoncrysol.2009.04.074.
[44] A. Hamdan, A. Hajimohammadi, A. Rawal, T. Kim, The intrinsic role of network modifiers (Ca versus Mg) in the reaction kinetics and microstructure of sodium silicate-activated CaO-MgO-Al2O3-SiO2 glasses, Cement Concr. Res. 164 (2023), https://doi.org/10.1016/j.cemconres.2022.107058.
[45] L.L. Hench, Bioceramics: from concept to clinic, J. Am. Ceram. Soc. 74 (1991) 1487–1510.
[46] J. Ma, C.Z. Chen, D.G. Wang, Y. Jiao, J.Z. Shi, Effect of magnesia on the degradability and bioactivity of sol-gel derived SiO2-CaO-MgO-P2O5 system glasses, Colloids Surf. B Biointerfaces 81 (2010) 87–95, https://doi.org/10.1016/j.colsurfb.2010.06.022.
[47] K. Sharma, C.B. Basak, M.N. Deo, M. Goswami, M. Krishnan, The effect of ZnO addition on thermo-physical and structural properties of 45S5 bioactive glass/glass-microspheres, in: AIP Conf. Proc., American Institute of Physics Inc., 2016, https://doi.org/10.1063/1.4947844.
[48] Q. Nawaz, A. de Pablos-Martín, J. Martins de Souza e Silva, K. Hurle, A.T. C. Jaimes, D.S. Brauer, A.R. Boccaccini, New insights into the crystallization process of sol-gel–derived 45S5 bioactive glass, J. Am. Ceram. Soc. 103 (2020) 4234–4247, https://doi.org/10.1111/jace.17124.
[49] M. Montazerian, A. Shearer, J.C. Mauro, Perspectives on the impact of crystallization in bioactive glasses and glass-ceramics, Int. J. Ceram. Eng. Sci. 6 (2024), https://doi.org/10.1002/ces2.10194.
[50] O.P. Filho, G.P. Latorre, L.L. Hench, Effect of crystallization on apatite-layer formation of bioactive glass 45%, J. Biomed. Mater. Res. 30 (1996) 509–514.
[51] M. Plewinski, K. Schickle, M. Lindner, A. Kirsten, M. Weber, H. Fischer, The effect of crystallization of bioactive bioglass 45S5 on apatite formation and degradation, Dent. Mater. 29 (2013) 1256–1264, https://doi.org/10.1016/j.dental.2013.09.016.
[52] S. De Micco, D. Bellucci, V. Cannillo, The assessment of bioactivity and biological responsiveness in bioactive glasses and ceramics: a review of available techniques, Materials 18 (2025) 4393, https://doi.org/10.3390/ma18184393.
[53] P. Li, C. Ohtsuki, T. Kokubo, K. Nakanishi, N. Soga, T. Nakamura, T. Yamamuro, Process of Formation of Bone-like Apatite Layer on Silica Gel, 1992.
[54] F. Baino, S. Yamaguchi, The use of simulated body fluid (SBF) for assessing materials bioactivity in the context of tissue engineering: review and challenges, Biomimetics 5 (2020) 1–19, https://doi.org/10.3390/biomimetics5040057.
[55] A. Dridi, K.Z. Riahi, S. Somrani, Mechanism of apatite formation on a poorly crystallized calcium phosphate in a simulated body fluid (SBF) at 37 °C, J. Phys. Chem. Solid. 156 (2021), https://doi.org/10.1016/j.jpcs.2021.110122.
[56] H. Wang, X. Hou, W. Zhang, D. Kong, Y. Zhou, The influencing mechanism of phosphorus component on network structure and bioactivity of bioactive glass, J. Mech. Behav. Biomed. Mater. 140 (2023), https://doi.org/10.1016/j.jmbbm.2023.105719.
[57] A. Moghanian, A. Sedghi, A. Ghorbanoghli, E. Salari, The effect of magnesium content on in vitro bioactivity, biological behavior and antibacterial activity of sol–gel derived 58S bioactive glass, Ceram. Int. 44 (2018) 9422–9432, https://doi.org/10.1016/j.ceramint.2018.02.159.
[58] R.L. Du, J. Chang, S.Y. Ni, W.Y. Zhai, J.Y. Wang, Characterization and in vitro bioactivity of zinc-containing bioactive glass and glass-ceramics, J. Biomater. Appl. 20 (2006) 341–360, https://doi.org/10.1177/0885328206054535.
[59] M.B. Taye, Biomedical applications of ion-doped bioactive glass: a review, Appl. Nanosci. (Switzerland) 12 (2022) 3797–3812, https://doi.org/10.1007/s13204-022-02672-7.
[60] D. Zhang, O. Leppäranta, E. Munukka, H. Ylänen, M.K. Viljanen, E. Eerola, M. Hupa, L. Hupa, Antibacterial effects and dissolution behavior of six bioactive glasses, J. Biomed. Mater. Res. 93 (2010) 475–483, https://doi.org/10.1002/jbm.a.32564.
[61] M. Diba, F. Tapia, A.R. Boccaccini, L.A. Strobel, Magnesium-containing bioactive glasses for biomedical applications, Int. J. Appl. Glass Sci. 3 (2012) 221–253, https://doi.org/10.1111/j.2041-1294.2012.00095.x.
[62] P. Stoor, E. Soderling, J.I. Salonen, Antibacterial effects of a bioactive glass paste on oral microorganisms, Acta Odontol. Scand. 56 (1998).
[63] Y. Liu, C. Chen, T. Liang, Y. Wang, R. Zhao, G. Li, C. Bai, Y. Wu, F. Yu, L. Sheng, R. Zhang, Y. Zhao, In vitro long-term antibacterial performance and mechanism of Zn-doped micro-arc oxidation coatings, Colloids Surf. B Biointerfaces 233 (2024), https://doi.org/10.1016/j.colsurfb.2023.113634.
[64] N. Azizabadi, P.A. Azar, M.S. Tehrani, P. Derakhshi, Synthesis and characteristics of gel-derived SiO2-CaO-P2O5-SrO-Ag2O-ZnO bioactive glass: bioactivity, biocompatibility, and antibacterial properties, J. Non. Cryst. Solids 556 (2021), https://doi.org/10.1016/j.jnoncrysol.2020.120568.
[65] Z. Atasayar, A. Akturk, D.N. Dikmetas, F. Karbancioglu-Guler, M. Erol-Taygun, S. Küçükbayrak, Fabrication of electrospun scaffolds with copper and zinc doped 58S bioactive glasses for bone tissue engineering applications, MRS Adv. 10 (2025) 1685–1693, https://doi.org/10.1557/s43580-024-01055-0.
[66] S. Sánchez-Salcedo, S. Shruti, A.J. Salinas, G. Malavasi, L. Menabue, M. Vallet-Regí, In vitro antibacterial capacity and cytocompatibility of SiO 2-CaO-P2O5 meso-macroporous glass scaffolds enriched with ZnO, J. Mater. Chem. B 2 (2014) 4836–4847, https://doi.org/10.1039/c4tb00403e.
[67] R.G. Hill, D.S. Brauer, Predicting the bioactivity of glasses using the network connectivity or split network models, J. Non. Cryst. Solids 357 (2011) 3884–3887, https://doi.org/10.1016/j.jnoncrysol.2011.07.025.
[68] J.R. Jones, Reprint of: review of bioactive glass: from Hench to hybrids, Acta Biomater. 23 (2015) S53–S82, https://doi.org/10.1016/j.actbio.2015.07.019.
[69] D.S. Brauer, Bioactive glasses - structure and properties, Angew. Chem. 127 (2015) 4232–4254, https://doi.org/10.1002/ange.201405310.